Power Spectra of Return-to-Zero Optical Signals

Ezra Ip and Joseph M. Kahn, *Fellow, IEEE*

Abstract—**Analytical formulas for the power spectra of return-to-zero (RZ) optical signals generated by Mach–Zehnder (MZ) modulators are derived. Pulse duty cycles of 33%, 50%, and 67%, in conjunction with several modulation techniques, including binary ON–OFF keying (OOK), duobinary OOK, and M-ary differential phase-shift keying (DPSK), phase-shift keying (PSK), and quadrature-amplitude modulation (QAM), are considered. Spectral characteristics and bandwidth requirements of these different schemes are compared.**

I. INTRODUCTION

RETURN-TO-ZERO (RZ) modulation formats are becoming increasingly popular for long-haul optical fiber transmission systems at bit rates of 10 Gb/s and above [1]. Previously, the benefits of RZ formats were often overlooked, because they require larger bandwidth than non-return-to-zero (NRZ) formats, and their generation typically requires two cascaded Mach–Zehnder (MZ) modulators. In recent years, it has been shown that RZ can have superior performance over NRZ in certain regimes where chromatic dispersion and fiber nonlinearities are present [2]–[4], as the RZ pulse may exhibit "soliton-like" properties. In addition, RZ has greater tolerance to polarization-mode dispersion than NRZ [5]. Recent research has compared the performance of RZ with different modulation techniques, including binary ON–OFF keying (OOK) and binary differential phase-shift keying (2-DPSK) [6], [7].

RZ pulses are frequently generated by driving an MZ modulator by a sinusoidal drive waveform; we assume throughout this paper that RZ pulses are generated in this manner. We define the pulse duty cycle as T_{FWHM}/T_S, where T_{FWHM} is the pulsewidth (full-width at half-maximum intensity), and T_S is the symbol duration. Depending on the drive waveform amplitude and bias, RZ pulses can have duty cycles of 33%, 50%, and 67%. In particular, 67% RZ is often referred to as carrier-suppressed RZ (CSRZ).

The optical power spectrum is an important characteristic of any modulation format to be employed in a dense wavelength-division-multiplexed (DWDM) system. The spectrum relates to several key system attributes, which include 1) optical filter bandwidth required for low distortion and crosstalk; 2) channel spacing required for low crosstalk; 3) sensitivity to chromatic dispersion; and 4) impact of fiber nonlinearity. (It should be pointed out that while the spectrum is indicative of these attributes, detailed performance analysis is required to precisely characterize these attributes for a given modulation scheme and system design.)

The spectra of various RZ schemes have been measured in several experiments [8], [9] and in numerous simulations. Since measured spectra can be corrupted by noise while simulated spectra can depend on the data sequence employed, it is desirable to compute the spectra analytically. While the spectra of nonoptical signals have been systematically analyzed [10], the spectra of externally modulated optical signals have not been fully characterized analytically. A major difficulty lies in the nonlinear transfer characteristic of the MZ modulator, which can cause the optical spectrum to be very different from the spectrum of the electrical drive signal. Recently, optical spectra were calculated for binary signals with both raised-cosine and Bessel-filtered NRZ pulse shapes and for optical duobinary signals created by Bessel-filtered NRZ pulse shape [11].

In this paper, we derive analytical formulas for the spectra of 33%, 50%, and 67% RZ, in conjunction with various modulation techniques, including binary OOK, duobinary OOK, and M-ary differential phase-shift keying (DPSK), phase-shift keying (PSK), and quadrature-amplitude modulation (QAM). We compare the spectral characteristics and bandwidth requirements of these schemes.

II. DERIVATION OF RZ POWER SPECTRA

We derive the spectra of modulated RZ data signals in this section. We review the generation of RZ data signals in part A and the time-domain waveforms of isolated RZ pulses in part B. In part C, we derive the frequency-domain spectra of isolated RZ pulses. In part D, we review the autocorrelation functions and power spectra of common modulation formats and combine the latter with the results of part C to obtain the power spectra of modulated RZ data signals.

A. Generation of Modulated RZ Data Signals

Throughout this paper, we assume that unchirped RZ signals are generated using a cascade of two MZ modulators, as shown in Fig. 1. We use $E(t)$ to denote a complex baseband electric field and $\hat{E}(f)$ to denote its Fourier transform. At each MZ modulator ($i = 1, 2$), the relationship between input and output electric fields satisfies

$$E_{i,\mathrm{out}}(t) = E_{i,\mathrm{in}}(t) \sin\left(\frac{\pi V_i(t)}{2V_\pi}\right). \tag{1}$$

For a balanced single-drive modulator, $V_i(t)$ represents the drive voltage. For a dual-drive modulator, $V_i(t)$ represents the algebraic difference between the two drive voltages, which
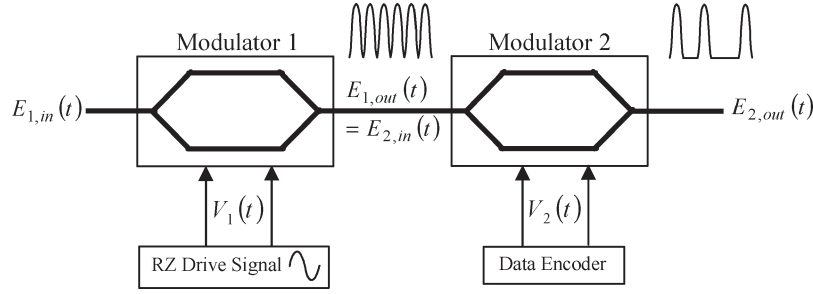
Fig. 1. Generation of RZ signals using cascaded MZ modulators. The output of the first modulator is a continuous stream of RZ pulses. The second modulator modulates the RZ pulse amplitudes in accordance with the modulation format.

must be complementary to produce zero chirp. For both modulator types, V_π represents the change in $V_i(t)$ that is required to swing the intensity from minimum to maximum.

We assume that the first modulator—known as the pulse carver—is driven by a sine wave $V_1(t)$ to produce an optical pulse train. The second modulator is driven with an NRZ electrical waveform $V_2(t)$ that encodes data onto the pulse train (Fig. 1). In this paper, we assume that the data encoder modulator has infinite modulation bandwidth. Assume that M-ary data symbols are encoded onto the pulse train. The interval between pulses, which is equal to the symbol interval T_s, is related to the bit interval T_b by

$$T_s = T_b \log_2 M. \tag{2}$$

Likewise, the pulse repetition rate, which is equal to the symbol rate R_s, is related to the bit rate R_b by

$$R_s = \frac{R_b}{\log_2 M}. \tag{2a}$$

In the particular case of binary transmission $M = 2$, we have $T_s = T_b$ and $R_s = R_b$.

B. Waveforms of Isolated RZ Pulses

A graphical representation of the sinusoidal drive voltage $V_1(t)$ required to produce 33%, 50%, and 67% RZ pulse trains is shown in Fig. 2. The underlying curve depicts the modulator transfer characteristic $E_{1,\mathrm{out}}(t)/E_{1,\mathrm{in}}(t)$ versus $V_1(t)$, given by (1), while the horizontal arrows denote the excursion of $V_1(t)$ over one cycle. In the case of 50% RZ, $V_1(t)$ passes through one intensity maximum per cycle, so the frequency of $V_1(t)$ equals the symbol rate R_s. In the cases of 33% and 67% RZ, $V_1(t)$ passes through two intensity maxima per cycle, so the frequency of $V_1(t)$ equals $R_s/2$. We note that in the cases of 33% and 50% RZ, $E_{1,\mathrm{out}}(t)/E_{1,\mathrm{in}}(t)$ is nonnegative over the excursion of $V_1(t)$, resulting in unipolar electric field waveforms. By contrast, in the case of 67% RZ, $E_{1,\mathrm{out}}(t)/E_{1,\mathrm{in}}(t)$ is both positive and negative over the excursion of $V_1(t)$, resulting in bipolar field waveforms that switch polarity between odd and even symbol intervals.

In this paper, we assume ideal RZ pulses produced by MZ modulators having infinite modulation bandwidth and zero
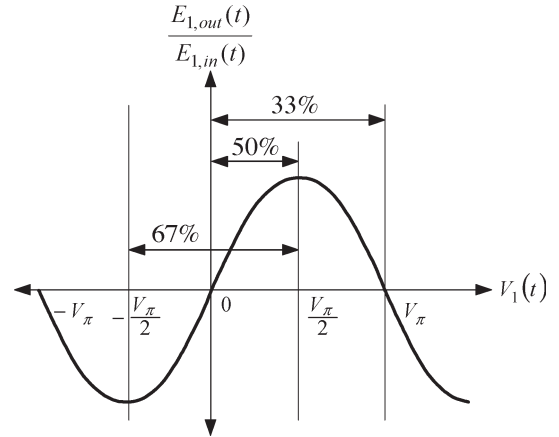

Fig. 2. Transfer characteristic of modulator 1, indicating the excursion of drive waveform $V_1(t)$ for generation of RZ pulse trains of 33%, 50%, and 67% duty cycles.

chirp.[1] We can write the time-domain electric field waveforms for isolated 33%, 50% and 67% RZ pulses as

$$E_{33}(t) = \begin{cases} \frac{1}{\sqrt{\mathsf{E}_{33}}} \sin\left(\frac{\pi}{2}\left[1 + \sin\left(\frac{\pi t}{T_s}\right)\right]\right), & -\frac{T_s}{2} \leq t \leq \frac{T_s}{2} \\ 0, & \text{otherwise} \end{cases} \tag{3}$$

$$E_{50}(t) = \begin{cases} \frac{1}{\sqrt{\mathsf{E}_{50}}} \sin\left(\frac{\pi}{4}\left[1 + \cos\left(\frac{2\pi t}{T_s}\right)\right]\right), & -\frac{T_s}{2} \leq t \leq \frac{T_s}{2} \\ 0, & \text{otherwise} \end{cases} \tag{4}$$

$$E_{67}(t) = \begin{cases} \frac{1}{\sqrt{\mathsf{E}_{67}}} \sin\left(\frac{\pi}{2}\cos\left(\frac{\pi t}{T_s}\right)\right), & -\frac{T_s}{2} \leq t \leq \frac{T_s}{2} \\ 0, & \text{otherwise} \end{cases} \tag{5}$$

---

[1] If chirp is significant, we can incorporate its effect by writing the chirped RZ pulses as

$$E_{i,\mathrm{chirp}}(t) = E_i(t) \cdot e^{j\alpha t^2}$$

where $E_{i,\mathrm{chirp}}(t)$ is a chirped pulse, $E_i(t)$ is the idealized pulse given by (3)–(5), and α is the chirp factor. The Fourier transform of the chirped pulse may be calculated by convolving the nonchirped pulse with the Fourier transform of the chirp term expressed as

$$\hat{E}_{i,\mathrm{chirp}}(f) = \hat{E}_i(f) \otimes \left[\sqrt{\frac{\pi}{\alpha}}\, e^{-j\pi^2 \frac{f^2}{\alpha^2}}\right]$$

where $\hat{E}_i(f)$ is given by (9)–(11). To compute the spectral broadening for a particular value of α, the above formula should be used in place of $\hat{E}_i(f)$ in (14).
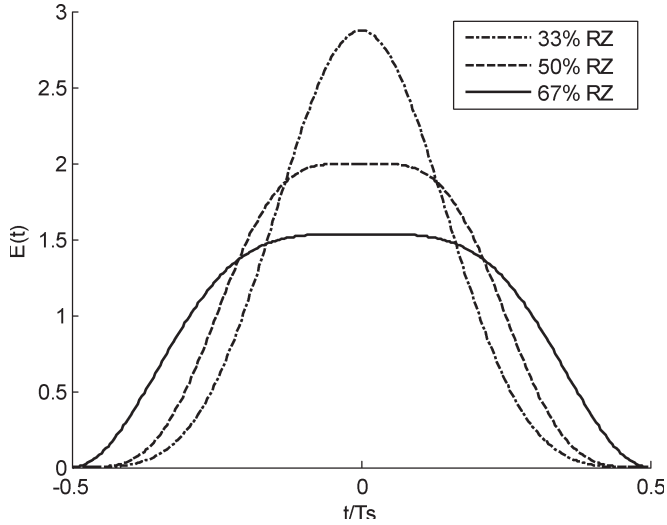
Fig. 3. Intensity waveforms of isolated 33%, 50%, and 67% RZ pulses. The pulses are normalized to have unit energy over the symbol period T_s.

where the pulse energies E_i are given by

$$\mathsf{E}_i = \int\limits_{-\infty}^{\infty} E_i^2(t)\, dt. \tag{6}$$

Recalling that 67% RZ is bipolar, we note that (5) provides the formula of a single RZ pulse in the positive polarity. It will be shown later that for spectra calculations, it is simpler to compute the Fourier transform of an isolated positive pulse and incorporate the polarity flip between odd and even symbols into the modulating data sequence. In Fig. 3, we plot the squared magnitudes of the RZ pulse waveforms given by (3)–(5). The pulses are normalized to have unit energy over the symbol period T_s.

C. Spectra of Isolated RZ Pulses

In order the compute the Fourier transform of an isolated RZ pulse, it is convenient to first periodically extend the isolated pulse to obtain a periodic pulse train having period T_s and then multiply the periodic pulse train by a rectangular function to extract an isolated RZ pulse.

For 33%, 50%, and 67% RZ, expressions for the isolated pulses $E_i(t)$ ($i = 33, 50, 67$) are given in (3)–(5). In order to obtain the corresponding periodically extended pulse trains $g_i(t)$, we simply remove the time constraints from (3)–(5), obtaining the expressions given in the second column of Table I. Using well-known expansions for sinusoidal functions of sinusoidal arguments [12], we represent the periodically extended pulse trains $g_i(t)$ as Fourier series with coefficients given by Bessel functions, as shown in the third column of Table I. We can then express these Fourier series as generalized Fourier transforms $\hat{g}_i(f)$ that are infinite sums of shifted impulses, as given in the fourth column of Table I.

In order to obtain an isolated pulse, we multiply a periodically extended pulse train $g_i(t)$ by a rectangular function, which

is expressed as

$$E_i(t) = g_i(t) \cdot h(t) \tag{7}$$

where

$$h(t) = \begin{cases} 1, & -\frac{T_s}{2} \le t \le \frac{T_s}{2} \\ 0, & \text{otherwise.} \end{cases} \tag{8}$$

This is illustrated in Fig. 4. Since multiplication by $h(t)$ in the time domain corresponds to convolution in the frequency domain by its Fourier transform $\hat{h}(f) = T_s \,\mathrm{sinc}\,(fT_s)$, the Fourier transform of an isolated RZ pulse is equal to an infinite sum of shifted sinc functions weighted by Bessel function coefficients $J_n(\beta)$

$$\hat{E}_{33}(f) = \frac{T_s}{\sqrt{\mathsf{E}_{33}}} \sum_{\substack{n=-\infty \\ n \text{ is even}}}^{\infty} J_n\left(\frac{\pi}{2}\right) \cdot \mathrm{sinc}\left(fT_s - \frac{n}{2}\right) \tag{9}$$

$$\hat{E}_{50}(f) = \frac{T_s}{\sqrt{2\mathsf{E}_{50}}} \sum_{n=-\infty}^{\infty} j^{n-\frac{1}{2}+\frac{1}{2}(-1)^n} J_n\left(\frac{\pi}{4}\right) \cdot \mathrm{sinc}(fT_s - n)$$

$$\tag{10}$$

$$\hat{E}_{67}(f) = \frac{T_s}{\sqrt{\mathsf{E}_{67}}} \sum_{\substack{n=-\infty \\ n \text{ is odd}}}^{\infty} j^{n-1} J_n\left(\frac{\pi}{2}\right) \cdot \mathrm{sinc}\left(fT_s - \frac{n}{2}\right). \tag{11}$$

In the above equations, $j = \sqrt{-1}$. Plots of the squared magnitudes of (9)–(11) are shown in Fig. 5.

D. Spectra of Modulated RZ Data Signals

In Fig. 1, the drive voltage $V_2(t)$ of the second MZ modulator causes a data symbol sequence $\{I_n\}_{n=-\infty}^{\infty}$ to be modulated onto the periodic RZ pulse train output from the first modulator. The data sequence I_n can be drawn from an arbitrary modulation format, e.g., OOK, DPSK, etc. We can write the output of the second modulator as

$$E_{2,\mathrm{out}}(t) = \sum_{n=-\infty}^{\infty} I_n \cdot E_i(t - nT_s) \equiv A(t). \tag{12}$$

In the remainder of the paper, to simply notation, we denote the output of the second modulator as $A(t)$. In (12), $E_i(t)$ is the electric field waveform of a single RZ pulse, given in (3)–(5) for the cases of 33%, 50%, and 67% RZ.

An autocorrelation function $\phi_{II}(m) = E\lfloor I_n^* I_{n+m}\rfloor$ exists for the data sequence. The spectrum of this autocorrelation function is defined as

$$\Phi_{II}(f) = \sum_{m=-\infty}^{\infty} \phi_{II}(m) \cdot e^{j2\pi mfT_s}. \tag{13}$$

Once the spectrum of the data sequence is found using (13), the complete baseband equivalent spectrum of the modulated RZ data signal can be computed as [10]

$$\Phi_{AA}(f) = \frac{1}{T_s} \Phi_{II}(f) \cdot \left|\hat{E}_i(f)\right|^2. \tag{14}$$

TABLE I
In Computing the Spectrum of an Isolated RZ Pulse, we Periodically Extend an Isolated Pulse and
Calculate the Fourier Transform of the Resulting Periodic Pulse Train

| RZ Pulse Duty Cycle	Periodically Extended Pulse Train $g_i(t)$	Periodically Extended Pulse Train as Fourier Series $g_i(t)$	Fourier Transform of Periodically Extended Pulse Train $\hat{g}_i(f)$
33%	$\dfrac{1}{\sqrt{E_{33}}}\sin\left(\dfrac{\pi}{2}\left[1+\sin\left(\dfrac{\pi t}{T_s}\right)\right]\right)$	$\dfrac{1}{\sqrt{E_{33}}}\displaystyle\sum_{\substack{n=-\infty \\ n-even}}^{\infty} J_n\left(\dfrac{\pi}{2}\right)\cdot e^{j\frac{\pi n t}{T_s}}$	$\dfrac{1}{\sqrt{E_{33}}}\displaystyle\sum_{\substack{n=-\infty \\ n-even}}^{\infty} J_n\left(\dfrac{\pi}{2}\right)\cdot\delta\left(f-\dfrac{n}{2T_s}\right)$
50%	$\dfrac{1}{\sqrt{E_{50}}}\sin\left(\dfrac{\pi}{4}\left[1+\cos\left(\dfrac{2\pi t}{T_s}\right)\right]\right)$	$\dfrac{1}{\sqrt{2E_{50}}}\displaystyle\sum_{n=-\infty}^{\infty} j^{n-\frac{1}{2}+\frac{1}{2}(-1)^n} J_n\left(\dfrac{\pi}{4}\right)\cdot e^{j\frac{2\pi n t}{T_s}}$	$\dfrac{1}{\sqrt{2E_{50}}}\displaystyle\sum_{n=-\infty}^{\infty} j^{n-\frac{1}{2}+\frac{1}{2}(-1)^n} J_n\left(\dfrac{\pi}{4}\right)\cdot\delta\left(f-\dfrac{n}{T_s}\right)$
67%	$\dfrac{1}{\sqrt{E_{67}}}\sin\left(\dfrac{\pi}{2}\cos\left(\dfrac{\pi t}{T_s}\right)\right)$	$\dfrac{1}{\sqrt{E_{67}}}\displaystyle\sum_{\substack{n=-\infty \\ n-odd}}^{\infty} j^{n-1} J_n\left(\dfrac{\pi}{2}\right)\cdot e^{j\frac{\pi n t}{T_s}}$	$\dfrac{1}{\sqrt{E_{67}}}\displaystyle\sum_{\substack{n=-\infty \\ n-odd}}^{\infty} j^{n-1} J_n\left(\dfrac{\pi}{2}\right)\cdot\delta\left(f-\dfrac{n}{2T_s}\right)$
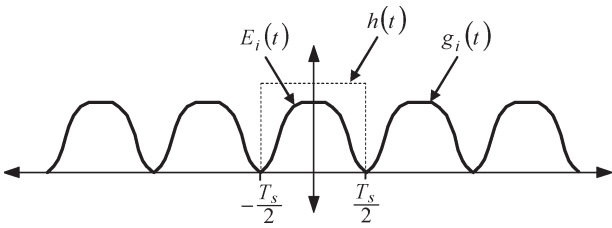
Fig. 4. Isolated RZ pulse $E_i(t)$ is obtained by multiplying its periodic extension $g_i(t)$ by $h(t)$.

According to (14), the spectrum of modulated RZ depends on the spectrum of the isolated pulse shape $\hat{E}_i(f)$ and the spectrum of the data sequence I_n. The autocorrelation functions and spectra of common modulation formats are shown in Table II [10]. In evaluating the spectra $\hat{E}_i(f)$ given by (9)–(11), we consider unit pulse energies $E_i = 1$. Hence, $\overline{P}$ represents the average power of the modulated RZ data signal.

There are two well-known methods of generating duobinary signals. In the first method, the second modulator's drive waveform $V_2(t)$ in Fig. 1 is produced by passing the input bit sequence through a delay-and-add circuit. The resulting waveform $V_2(t)$ is three leveled [10], [13]. In the second method, the drive waveform $V_2(t)$ is obtained by lowpass filtering a binary waveform, resulting in a quasi-three-level drive waveform [14]. In this paper, for analytical convenience, we consider the first type of duobinary encoder, i.e., the delay-and-add circuit.

As pointed out earlier, in the case of 67% RZ (CSRZ), the electric field waveform at the first MZ modulator's output (see Fig. 1) switches polarity between odd and even symbol intervals. For analytical convenience, we work with a unipolar field waveform and incorporate the polarity flips by inserting appropriate sign changes in the modulating data. Let I_n be the nth data symbol modulating the second MZ modulator. We may write a modified data sequence as

$$\bar{I}_n = (-1)^n I_n. \qquad (15)$$

The modulated RZ data signal is then the product of the modified data sequence $\bar{I}_n$ and the unipolar 67% RZ pulse train, whose single-pulse Fourier transform was computed in (11). The modified data sequence $\bar{I}_n$ has autocorrelation function

$\phi_{\overline{II}}(m)$ and spectrum $\Phi_{\overline{II}}(f)$. In order to compute the baseband equivalent spectrum of data signals with 67% RZ pulses, we use (14), substituting $\Phi_{\overline{II}}(f)$ for $\Phi_{II}(f)$.

The particular case of 67% RZ pulses with binary OOK is illustrated in Fig. 6. The modified data sequence $\bar{I}_n$ has an autocorrelation function $\phi_{\overline{II}}(m) = (-1)^m E[I^*_{\text{OOK},n} I_{\text{OOK},n+m}]$ given by

$$\phi_{\overline{II}}(m) = \begin{cases} \overline{P}, & m = 0 \\ \dfrac{\overline{P}}{2}, & m \neq 0,\ m \text{ is even} \\ \dfrac{-\overline{P}}{2}, & m \neq 0,\ m \text{ is odd.} \end{cases} \qquad (16)$$

The spectrum of this modified data sequence can be shown to equal

$$\Phi_{\overline{II}}(f) = \frac{\overline{P}}{2} + \frac{\overline{P}}{2T_s}\sum_{\substack{n=-\infty \\ n \text{ is odd}}}^{\infty} \delta\left(f - \frac{n}{2T_s}\right). \qquad (17)$$

In the case of 67% RZ pulses with duobinary OOK, we consider a delay-and-add duobinary encoder (the first method described above), as we have considered for 33% and 50% RZ. The modified data sequence $\bar{I}_n$ has a power spectrum given by

$$\Phi_{\overline{II}}(f) = \overline{P} - \overline{P}\cos(2\pi f T_s). \qquad (18)$$

Note that [15] proposed a 67% RZ duobinary OOK scheme using a lowpass filter duobinary encoder (the second method described above).

In the cases of 67% RZ pulses with DPSK, PSK, or QAM, the original data sequence I_n and modified data sequence $\bar{I}_n$ have identical autocorrelation functions and thus identical spectra.

III. Results and Simulations

Figs. 7–9 show the baseband equivalent power spectra for 33%, 50%, and 67% RZ when various modulation schemes are employed. In Figs. 7–9, the frequency scale is expressed in terms of $fT_s = f/R_s$, where the symbol duration T_s and symbol rate R_s are given by (2) and (2a). Because M-ary modulation uses a symbol rate R_s that is $\log_2 M$ lower than the bit rate R_b, M-ary modulation is $\log_2 M$ times more bandwidth efficient than binary $(M = 2)$ modulation.
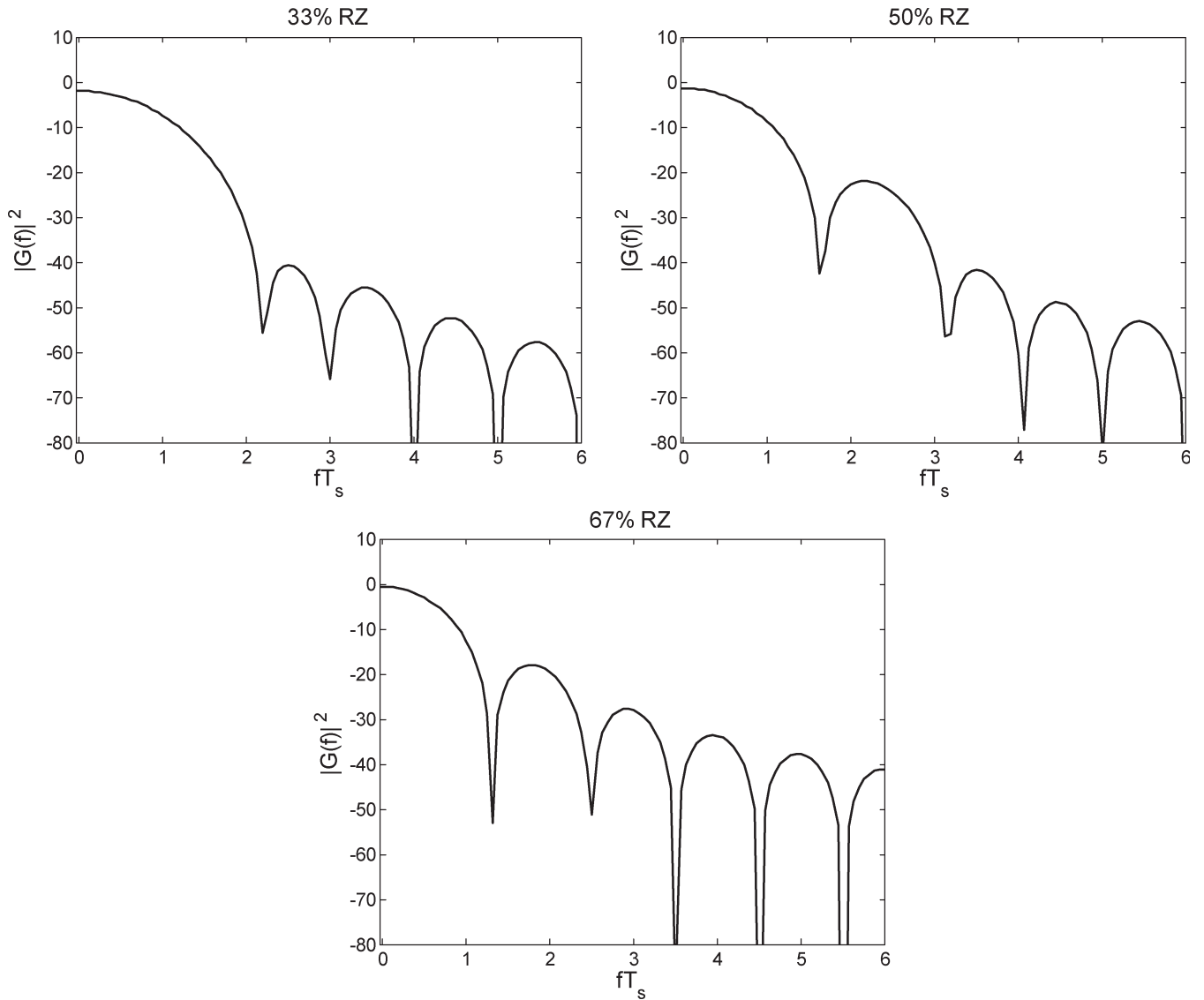
Fig. 5.   Squared magnitudes of Fourier transforms of isolated 33%, 50%, and 67% RZ pulses.

TABLE II

AUTOCORRELATION FUNCTIONS AND SPECTRA OF COMMON DIGITAL MODULATION FORMATS. $\overline{P}$ REPRESENTS THE AVERAGE POWER OF THE MODULATED RZ DATA SIGNAL, PROVIDED THAT THE PULSE ENERGY E_i, GIVEN BY (6), IS SET TO UNITY

Modulation Format	Autocorrelation Function $\phi_{II}(m)$	Spectrum $\Phi_{II}(f)$
Binary OOK	$\phi_{II}(m) = \begin{cases} \overline{P} & m = 0 \\ \overline{P}/2 & m \neq 0 \end{cases}$	$\Phi_{II}(f) = \dfrac{\overline{P}}{2}\left(1 + \dfrac{1}{T_s}\sum_{n=-\infty}^{\infty}\delta\left(f - \dfrac{n}{T_s}\right)\right)$
Duobinary OOK	$\phi_{II}(m) = \begin{cases} \overline{P} & m = 0 \\ \overline{P}/2 & m = \pm 1 \\ 0 & else \end{cases}$	$\Phi_{II}(f) = \overline{P} + \overline{P}\cos(2\pi f T_s)$
M-ary DPSK, PSK or QAM	$\phi_{II}(m) = \begin{cases} \overline{P} & m = 0 \\ 0 & m \neq 0 \end{cases}$	$\Phi_{II}(f) = \overline{P}$

The theoretical plots in Figs. 7–9 display strong agreement with available experimentally measured spectra [8], [9], [15]. We have also verified the theoretical plots in Figs. 7–9 by Monte Carlo simulations. The simulations were performed by generating a random sequence of 1024 modulated RZ symbols and then oversampling the signal at 64 times the symbol rate. We estimated the signal's spectrum using the periodogram technique, dividing the modulated RZ output into blocks of 16 symbols, and computing an average spectrum of the blocks. Essentially perfect matching between theory and simulation
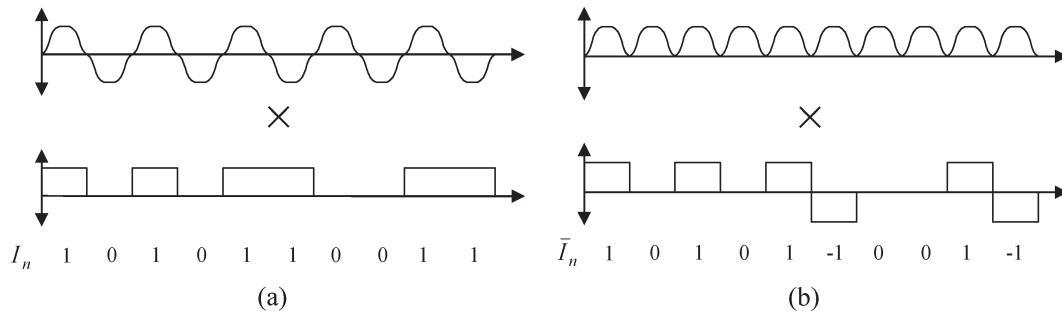
Fig. 6. Generation of 67% RZ (CSRZ) signals with OOK. (a) Actual implementation: a bipolar pulse train is modulated by a unipolar data sequence I_n. (b) Equivalent model used for analysis: a unipolar pulse train is modulated by a bipolar data sequence $\bar{I}_n = (-1)^n I_n$.
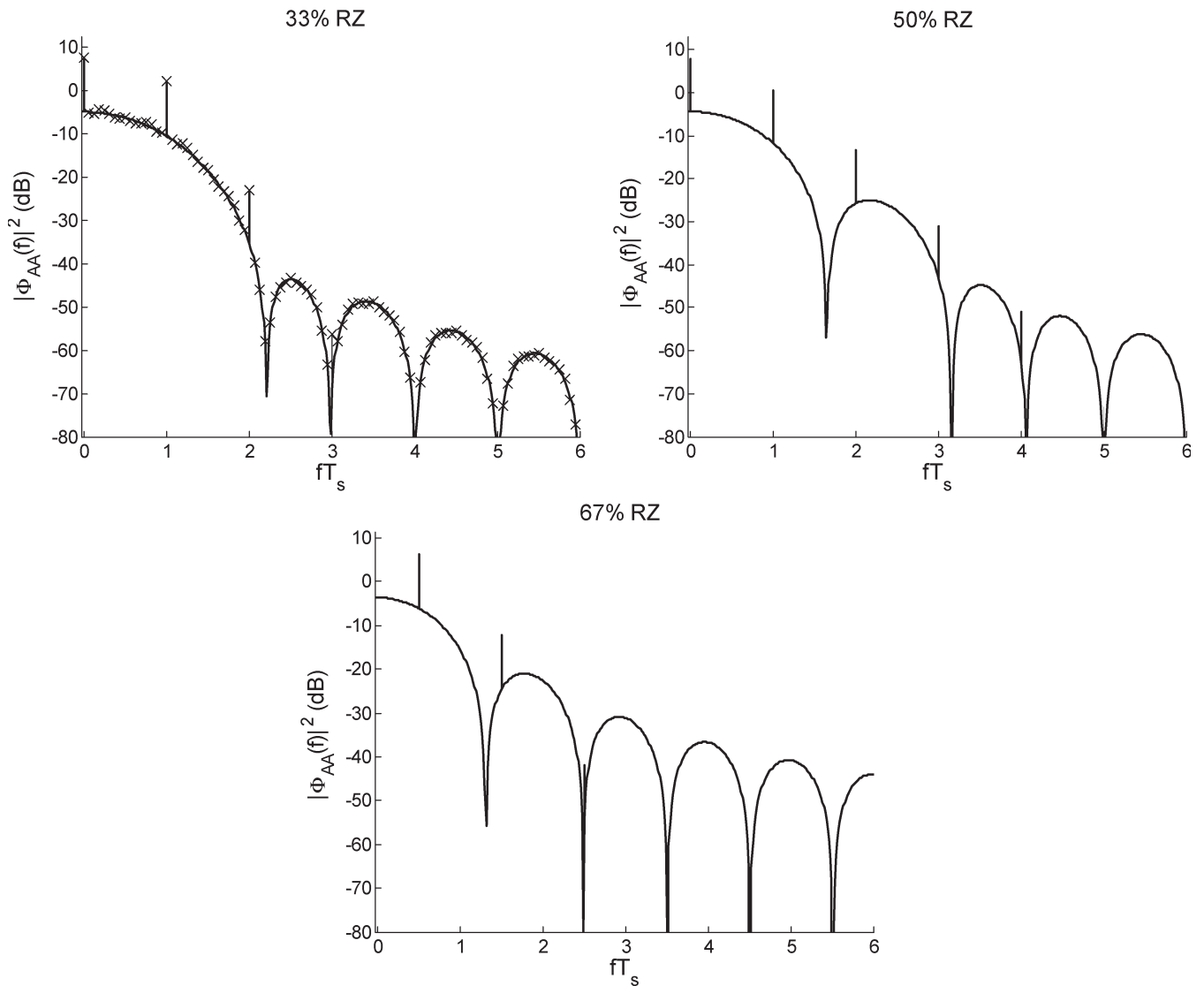

Fig. 7. Spectra of RZ signals with binary OOK. Solid line: analytical formula, x: Monte Carlo simulation.

results was observed in all cases. In the first plot of Fig. 7, we display the theoretical spectrum as a solid line, and the simulation results as discrete crosses. In all the other cases, we display only the theoretical results.

A major reason for computing the spectrum of a data signal is to determine the signal's bandwidth. We use the following expression to define a bandwidth $B(\gamma)$ around the carrier frequency over which a given fraction γ of the total energy is contained:

$$\gamma = \frac{\int_{-\frac{B(\gamma)}{2}}^{\frac{B(\gamma)}{2}} |\Phi_{AA}(f)|^2 \, df}{\int_{-\infty}^{\infty} |\Phi_{AA}(f)|^2 \, df}. \tag{19}$$
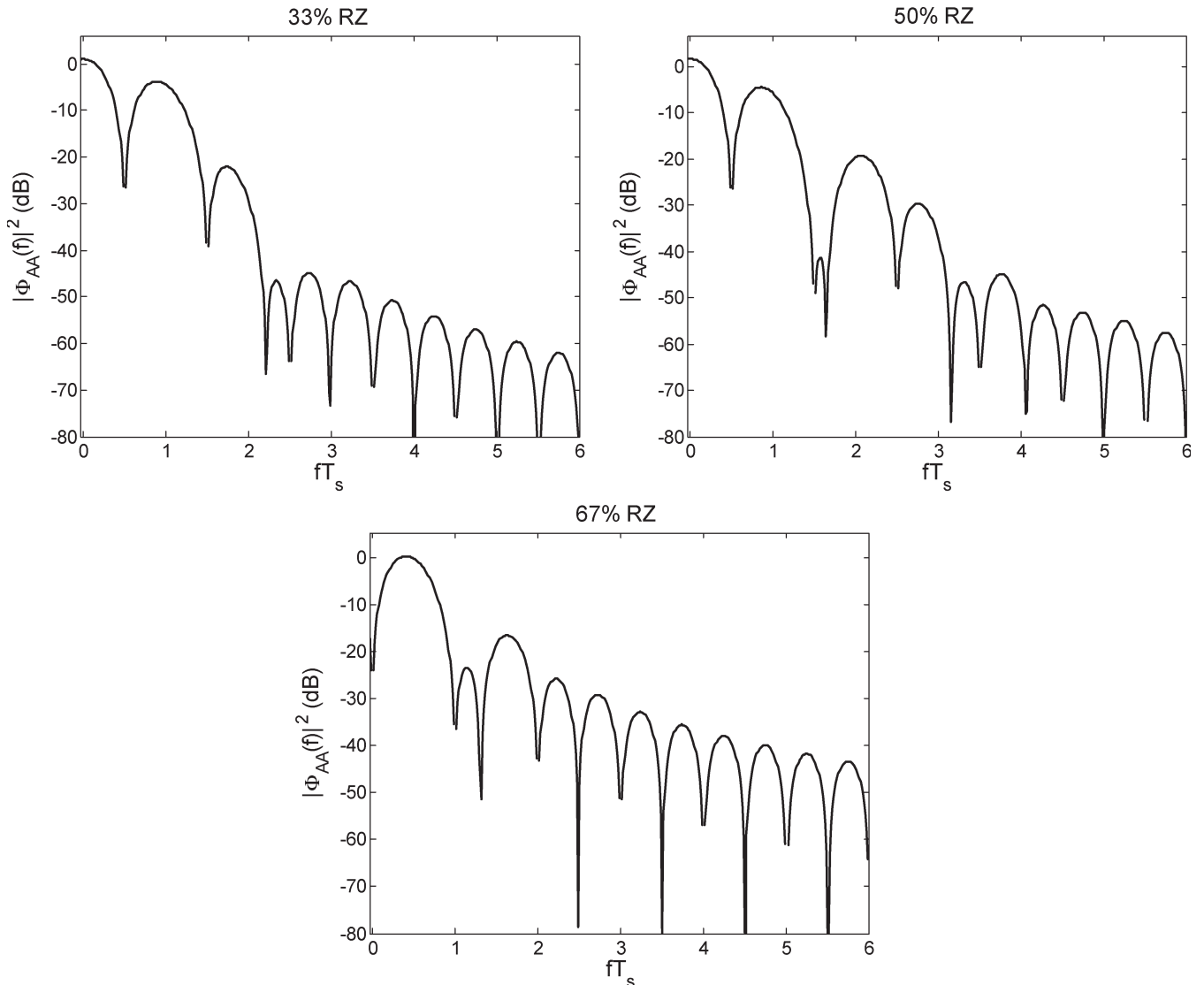
Fig. 8.   Spectra of RZ signals with duobinary OOK.

The integration in (19) is performed over a range centered at $f = 0$, because (14) represents a baseband equivalent spectrum.

Table III lists the bandwidths $B(\gamma)$ containing 90% and 99% of the total power for the different RZ modulation schemes. We note from Fig. 7 that the OOK spectra have impulses at frequencies equal to integer multiples of the symbol period. Half of the power of an OOK signal lies in these impulses. We computed two bandwidths for OOK in Table III, first with the impulses included in our calculations and then without. The results with the impulses considered are shown in parentheses in the first row of Table III. The results without the impulses are shown without parentheses and are observed to be the same as the bandwidths for M-ary DPSK, PSK, or QAM.

IV. DISCUSSION

The spectra plotted in Figs. 7–9 reveal a number of features that are discussed in this section.

Among all the modulation formats considered here, binary OOK with 33% and 50% RZ are unique in having an impulse in the spectrum at the carrier frequency, which results from the nonzero mean of the data sequence I_n [10]. In the case of binary OOK with 67% RZ (CSRZ), the periodic alternation of the pulse polarity (or of the modified data sequence $\bar{I}_n$) shifts the spectral impulses to half the symbol rate above and below the carrier frequency ($f = \pm 1/2T_s$ in Fig. 7) [15]. In the case of all other modulation formats, the absence of the impulse at the carrier frequency can be attributed to the zero mean of the data sequence I_n [10].

Fourier transform theory indicates that the shorter the duration of a signal in time, the wider its bandwidth in frequency. A comparison of the main lobes of Fig. 5 confirms this: The RZ pulse that has the shortest time duration (33% RZ) has the widest main lobe, whereas the pulse with the longest time duration (67% RZ) has the narrowest main lobe.

When computing signal bandwidths based on the containment of a given percentage of total power, we find the heights of the side lobes to be very important. Considering signal bandwidths that contain 90% of the total power, there is a monotonic decrease in bandwidth as the duty cycle progresses from 33%
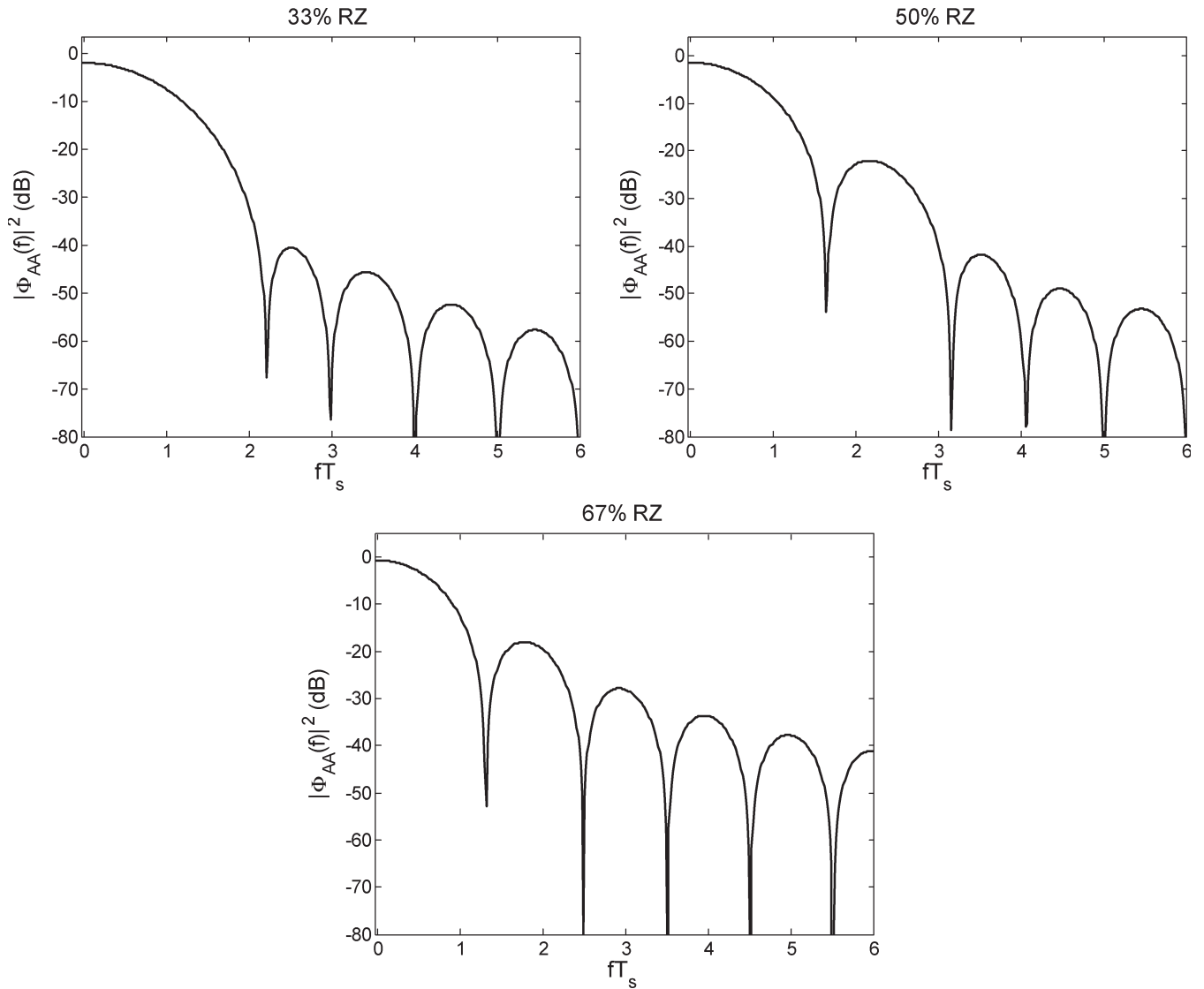
Fig. 9. Spectra of RZ signals with M-ary DPSK, PSK, or QAM.

TABLE III
BANDWIDTHS $B(\gamma)$ IN WHICH 90% AND 99% OF THE TOTAL POWER IS CONTAINED FOR VARIOUS RZ MODULATION SCHEMES. FOR BINARY OOK, BANDWIDTHS NOT IN PARENTHESES DO NOT INCLUDE THE IMPULSES IN THE POWER SPECTRA, WHILE THOSE IN PARENTHESES INCLUDE THE IMPULSES

	33% RZ		50% RZ		67% RZ	
	90% Bandwidth	99% Bandwidth	90% Bandwidth	99% Bandwidth	90% Bandwidth	99% Bandwidth
Binary OOK	$\dfrac{2.00}{T_s}\left(\dfrac{2.00}{T_s}\right)$	$\dfrac{2.97}{T_s}\left(\dfrac{2.75}{T_s}\right)$	$\dfrac{1.75}{T_s}\left(\dfrac{2.00}{T_s}\right)$	$\dfrac{2.84}{T_s}\left(\dfrac{2.97}{T_s}\right)$	$\dfrac{1.47}{T_s}\left(\dfrac{1.66}{T_s}\right)$	$\dfrac{3.69}{T_s}\left(\dfrac{4.00}{T_s}\right)$
Duobinary OOK	$\dfrac{2.06}{T_s}$	$\dfrac{2.59}{T_s}$	$\dfrac{1.94}{T_s}$	$\dfrac{2.72}{T_s}$	$\dfrac{1.34}{T_s}$	$\dfrac{3.28}{T_s}$
M-ary DPSK, PSK or QAM	$\dfrac{2.00}{T_s}$	$\dfrac{2.97}{T_s}$	$\dfrac{1.75}{T_s}$	$\dfrac{2.84}{T_s}$	$\dfrac{1.47}{T_s}$	$\dfrac{3.69}{T_s}$

to 50% to 67%, as one might expect. Considering bandwidths containing 99% of the power, however, 67% RZ actually has a wider bandwidth than 33% RZ for each modulation format. In the isolated pulse spectra shown in Fig. 5, we note that the side lobes increase in height as the duty cycle is increased from 33%

to 67%, and 67% RZ has a larger percentage of its total power contained in the side lobes.

Another observation is that the presence of nulls inside the main lobe can have an unexpected effect on the band-width. Duobinary encoding is normally used to reduce signal

bandwidth. Duobinary encoding can actually reduce the proportion of energy that exists inside the main lobe, which may be evident in a careful comparison between Figs. 7 and 8. Consequently, the 90% bandwidth for duobinary OOK is actually larger than the 90% bandwidth for binary OOK, for both 33% and 50% RZ.

It is clear from the above discussion that bandwidth comparisons between different RZ signals depend on the criterion used (e.g., 90% versus 99%) and must be evaluated on a case-by-case basis.

Finally, we remind the reader that while the spectral characteristics of a modulation scheme are indicative of key DWDM system performance attributes, including filter distortion, crosstalk, chromatic dispersion, and fiber nonlinearity, detailed performance analysis is required to precisely characterize these attributes for any particular modulation format and system design.

V. CONCLUSION

In this paper, we derived analytical formulas for the spectra of modulated RZ data signals with various pulse duty cycles and modulation formats. We found that the width of the main spectral lobe decreases as the duty cycle progresses from 33% to 50% to 67%. However, this is accompanied by an increase in the power contained in the spectral side lobes. We determined bandwidths of RZ signals that contain 90% or 99% of the total power. We found that in determining the bandwidth containing a high percentage of the power (e.g., 99%), the power in the side lobes becomes important. We also found that duobinary encoding may not necessarily decrease a signal's bandwidth. The criteria for evaluating the suitability of an RZ scheme need to be carefully matched to the requirements of a particular system.

REFERENCES

[1] A. Sahara, T. Inui, T. Komukai, H. Kubota, and M. Nakazawa, "40-Gb/s RZ transmission over a transoceanic distance in a dispersion managed standard fiber using a modified inline synchronous method," *J. Lightw. Technol.*, vol. 18, no. 10, pp. 1364–1373, Oct. 2000.

[2] M. I. Hayee and A. E. Willner, "NRZ versus RZ in 10–40-Gb/s dispersion-managed WDM transmission systems," *IEEE Photon. Technol. Lett.*, vol. 11, no. 8, pp. 991–993, Aug. 1999.

[3] C. Caspar, H. M. Foisel, A. Gladisch, N. Hanik, F. Küppers, R. Ludwig, A. Mattheus, W. Pieper, B. Strebel, and H. G. Weber, "RZ versus NRZ modulation format for dispersion compensated SMF-based 10 Gb/s transmission with more than 100-km amplifier spacing," *IEEE Photon. Technol. Lett.*, vol. 11, no. 4, pp. 991–993, Apr. 1999.

[4] D. Breuer and K. Petermann, "Comparison of NRZ- and RZ-modulation format for 40-Gb/s TDM standard-fiber systems," *IEEE Photon. Technol. Lett.*, vol. 9, no. 3, pp. 398–400, Mar. 1997.

[5] H. Sunnerud, M. Karlsson, and P. A. Andrekson, "A comparison between NRZ and RZ data formats with respect to PMD-induced system degradation," *IEEE Photon. Technol. Lett.*, vol. 13, no. 5, pp. 448–450, May 2001.

[6] T. Mizuochi, K. Ishida, T. Kobayashi, J. Abe, K. Kinjo, K. Motoshima, and K. Kasahara, "A comparative study of DPSK and OOK WDM transmission over transoceanic distances and their performance degradations due to nonlinear phase noise," *J. Lightw. Technol.*, vol. 21, no. 9, pp. 1933–1943, Sep. 2003.

[7] C. Xu, X. Liu, L. Mollenauer, and X. Wei, "Comparison of return-to-zero differential phase-shift keying and ON–OFF keying in long-haul dispersion managed transmission," *IEEE Photon. Technol. Lett.*, vol. 15, no. 4, pp. 617–619, Apr. 2003.

[8] A. Hodižić, B. Konrad, and K. Petermann, "Alternative modulation formats in $N \times 40$ Gb/s WDM standard fiber RZ-transmission systems," *J. Lightw. Technol.*, vol. 20, no. 4, pp. 598–607, Apr. 2002.

[9] Y. Kisaka, M. Tomizawa, A. Hirano, S. Kuwahara, and Y. Miyamoto, "Compact-spectrum RZ signal generated by single-stage push–pull type Mach–Zehnder modulator for DWDM transmission," *Electron. Lett.*, vol. 39, no. 3, pp. 304–306, Feb. 2003.

[10] J. G. Proakis, *Digital Communications*, 4th ed. New York: McGraw-Hill, 2002.

[11] K.-P. Ho and J. M. Kahn, "Spectrum of externally modulated optical signals," *J. Lightw. Technol.*, vol. 22, no. 2, pp. 658–663, Feb. 2004.

[12] M. Abramowitz and I. A. Stegun, *Handbook of Mathematical Functions*. New York: Wiley, 1993. Reprint Edition.

[13] K. Yonenaga, S. Kuwano, S. Norimatsu, and N. Shibata, "Optical duobinary transmission system with no receiver sensitivity degradation," *Electron. Lett.*, vol. 31, no. 4, pp. 302–304, Feb. 1995.

[14] T. Ono, Y. Yano, and K. Fukuchi, "Demonstration of high-dispersion tolerance of 20-Gb/s optical duobinary signal generated by a low-pass filtering method," in *Proc. Optical Fiber Communication (OFC)*, Dallas, TX, 1997, pp. 268–269.

[15] D. Lee, M. Lee, Y. Wen, and A. Nirmalathas, "A simple configuration to generate 40 Gbit/s duobinary CSRZ and CSRZ-DPSK signals with enlarged dispersion tolerance," in *Proc. 16th Annu. Meeting IEEE LEOS*, Tucson, AZ, Oct. 2003, vol. 1, pp. 26–30.

Ezra Ip received the B.E. (Hons) degree in electrical and electronics engineering from the University of Canterbury, Canterbury, U.K., in 2002 and the M.S. degree in electrical engineering from Stanford University, Stanford, CA, in 2004. He is currently working toward the Ph.D. degree in electrical engineering at Stanford University.

In 2002, he was a research engineer at Industrial Research Ltd., New Zealand. His research interests include single mode optical fiber communications.

Joseph M. Kahn (F'00) received the A.B., M.A., and Ph.D. degrees in physics from the University of California, Berkeley (U.C. Berkeley) in 1981, 1983, and 1986, respectively.

From 1987 to 1990, he was at AT&T Bell Laboratories, Crawford Hill Laboratory, Holmdel, NJ. He demonstrated multi-Gb/s coherent optical fiber transmission systems, setting world records for receiver sensitivity. From 1990 to 2003, he was on the faculty of the Department of Electrical Engineering and Computer Sciences at U.C. Berkeley, performing research on optical and wireless communications. Since 2003, he has been a Professor of electrical engineering at Stanford University, Stanford, CA. His current research interests include single- and multimode optical fiber communications, free-space optical communications, and MEMS for optical communications.

Prof. Kahn received the National Science Foundation Presidential Young Investigator Award in 1991. From 1993 to 2000, he served as a Technical Editor of *IEEE Personal Communications Magazine*. In 2000, he helped found StrataLight Communications, where he served as Chief Scientist from 2000 to 2003.